Stability and dynamical property for two-species ultracold atoms in double wells

Xiao-Qiang Xu, Li-Hua Lu, and You-Quan Li
Zhejiang Institute of Modern Physics and Department of Physics, Zhejiang University, Hangzhou 310027, People's Republic of China
(Received 9 June 2008; published 14 October 2008)

We study undistinguishable two-species Bose-Einstein condensates (BECs) trapped in double wells. In the mean-field approximation we map the quantum system into a classical model and investigate the existence and stability of the fixed point solutions. By appropriately varying the amplitude of the high-frequency periodic modulation on the energy bias between the two wells, we tune the tunneling strength in the adiabatic Rosen-Zener type effectively. Starting from two typical initial states, we study the evolution of the system and find that the interspecies interaction can produce totally distinct results, which is expected to provide a route to manipulate the BEC distribution.

DOI: 10.1103/PhysRevA.78.043609 PACS number(s): 03.75.Lm, 03.75.Mn, 03.75.Kk

I. INTRODUCTION

Bose-Einstein condensates (BECs) in double wells offer a powerful tool to study the quantum tunneling phenomena [1] since almost every parameter can be tuned experimentally, i.e., the interwell tunneling strength, on-site interaction strength, and also the energy bias between the two wells. There have been extensive studies on the single-species BEC in double wells in recent years. The most prominent feature of its tunneling is the nonlinear dynamics arising from the interaction between atoms. Several phenomena like self-trapping (ST) and Josephson oscillation (JO) [2–4] were observed in experiments recently [5]. Such a quantum system can be mapped into a classical Hamiltonian which gives rise to fixed-point solutions. The emergence of phenomena ST and JO are strongly related to these fixed point solutions. This is because there is a correspondence between the quantum eigenstates and the classical fixed points [6]. However, if the initial state of the system is merely a fixed point, it will keep "fixed" and never evolve [7]. If the tunneling strength is tuned adiabatically, the system will evolve due to the shift of fixed points. The complete population transfer between the two wells may occur for the adiabatic Rosen-Zener form of tunneling strength [9], which was originally proposed in Ref. [8] to study the spin-flip problem of two-level atoms. Compared with other forms of tunneling, such as the monotonic ones, this result may be natural. However, it is somewhat counterintuitive for Rosen-Zener form since the initial and final tunneling strengths are the same. There are several ways to tune the tunneling strength, e.g., by changing the distance between the two wells or the height of the potential barrier separating the two wells. Additionally, the tunneling strength can also be effectively tuned through periodically modulating the energy bias between the wells [10–12].

In comparison to the single-species case, the multispecies BECs exhibit richer physics due to the existence of the interspecies interaction. Previous studies focus on the equilibrium properties of the system, e.g., the component separation [13,14], the cancelation of the mean-field energy shift [15], etc. When trapped in double wells, the tunneling process owns more new features, e.g., quantum-correlated tunneling between the two species [16], the renewed macroscopic JO and ST effects [17,18], and the spin tunneling [19,20], etc. In this paper we consider an undistinguishable two-species BEC system confined in double wells. We study its adiabatic dynamical properties with the application of a high-frequency periodic modulation on energy bias between the wells which has never been studied before. In the next section, we employ the mean-field approximation to map the quantum model into a classical Hamiltonian and derive the corresponding dynamical equations. In Sec. III, we solve the fixed points and discuss their stabilities. In Sec. IV, we give the numerical results where two typical initial states are considered, respectively. Our results are briefly summarized and discussed in Sec. V.

II. MODELING THE SYSTEM

We consider a two-species Bose-Einstein condensate system trapped in double wells. The Hamiltonian of such a system is given by

$$H = -\sum_{\sigma} (J_{\sigma}\hat{c}^{\dagger}_{\sigma 1}\hat{c}_{\sigma 2} + \text{H.c.}) + \sum_{\sigma,\sigma',i} \frac{1}{2}\tilde{U}_{\sigma\sigma'}\hat{n}_{\sigma i}\hat{n}_{\sigma' i} - \sum_{\sigma,i} \frac{1}{2}\tilde{U}_{\sigma\sigma}\hat{n}_{\sigma i}, \tag{1}$$

where $\hat{c}^{\dagger}_{\sigma i}$ ($\hat{c}_{\sigma i}$) creates (annihilates) a boson of species σ in the ith well, and $\hat{n}_{\sigma i}=\hat{c}^{\dagger}_{\sigma i}\hat{c}_{\sigma i}$ denotes the particle number operator. Here the subscripts i ($i=1,2$) specify the two wells while σ ($\sigma=a,b$) refer to two different species whose interwell tunneling strengths are denoted by J_a and J_b, respectively; $\tilde{U}_{aa}$ and $\tilde{U}_{bb}$ are the intraspecies interaction strength while $\tilde{U}_{ab}$ the interspecies interaction strength. Such a two-species BEC mixture may consist of different atoms, or different isotopes, or different hyperfine states of the same kind of atom.

In order to investigate the dynamical properties of the system, we need to work with the equations of motion. In the

mean-field approximation $\langle \hat{c}_{\sigma i} \rangle = c_{\sigma i}$ with $c_{\sigma i}$ being c numbers, the Heisenberg equations give rise to the following equations:

$$i\dot{c}_{\sigma i} = -J_\sigma c_{\sigma \bar{i}} + U_\sigma |c_{\sigma i}|^2 c_{\sigma i} + U_{\sigma\bar{\sigma}} |c_{\bar{\sigma} i}|^2 c_{\sigma i}, \tag{2}$$

where $U_\sigma = \tilde{U}_{\sigma\sigma} N$ and $U_{\sigma\bar{\sigma}} = \tilde{U}_{\sigma\bar{\sigma}} N$ with N being the particle number of each species ($N_a = N_b = N$ for simplicity). Here the overhead dot denotes the time derivative and $\hbar$ is set to unit. Note that σ and $\bar{\sigma}$ refer to different species while i and $\bar{i}$ to different wells. Equation (2) is the well-known Gross-Pitaevskii equation.

We further express $c_{\sigma i}$ as $\sqrt{\rho_{\sigma i}} e^{i\theta_{\sigma i}}$ and define $\phi_\sigma = \theta_{\sigma 2} - \theta_{\sigma 1}$, $z_\sigma = \rho_{\sigma 1} - \rho_{\sigma 2}$ with $\rho_{\sigma i}$ and $\theta_{\sigma i}$ being the distribution probability and phase of species σ in the ith well, respectively. The conservation of particle numbers of each species requires $\rho_{a1} + \rho_{a2} = 1$ and $\rho_{b1} + \rho_{b2} = 1$. Since ϕ_σ and z_σ are mutually canonical conjugations, the equations of motion can be rewritten as

$$\dot{\phi}_a = J_a \cos\phi_a \frac{2z_a}{\sqrt{1 - z_a^2}} + U_a z_a + U_{ab} z_b,$$

$$\dot{z}_a = -2J_a \sin\phi_a \sqrt{1 - z_a^2},$$

$$\dot{\phi}_b = J_b \cos\phi_b \frac{2z_b}{\sqrt{1 - z_b^2}} + U_b z_b + U_{ab} z_a,$$

$$\dot{z}_b = -2J_b \sin\phi_b \sqrt{1 - z_b^2}, \tag{3}$$

and the corresponding classical Hamiltonian is given by

$$H_{mf} = -2J_a \cos\phi_a \sqrt{1 - z_a^2} + \frac{1}{2} U_a z_a^2 - 2J_b \cos\phi_b \sqrt{1 - z_b^2} + \frac{1}{2} U_b z_b^2 + U_{ab} z_a z_b. \tag{4}$$

In the following, we only consider the case $U_a = U_b = U$, $J_a = J_b = J$ for simplicity [21]. We also assume positive U, U_{ab}, and J and take $U_{ab} \leqslant U$ so that the miscibility condition [13] is fulfilled.

III. FIXED POINTS AND THEIR STABILITY

The adiabatic evolution of quantum eigenstates corresponds to the movement of fixed points determined by the classical Hamiltonian. In order to get the fixed point solutions, we set $\dot{\phi}_\sigma = 0$, $\dot{z}_\sigma = 0$ in Eqs. (3) and obtain

$$z_a = -\frac{1}{U_{ab}} \left(\frac{2J}{\sqrt{1 - z_b^2}} \xi_b + U \right) z_b,$$

$$z_b = -\frac{1}{U_{ab}} \left(\frac{2J}{\sqrt{1 - z_a^2}} \xi_a + U \right) z_a, \tag{5}$$

with $\xi_a = \cos\phi_a$ and $\xi_b = \cos\phi_b$ where ϕ_a and ϕ_b are either 0 or π.

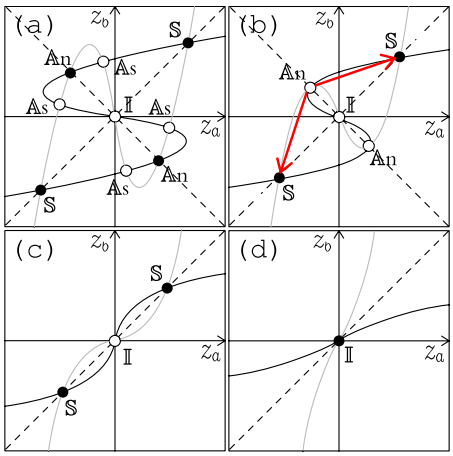

FIG. 1. (Color online) Equations (5) plotted for different values of U, U_{ab}, and J in the (z_a, z_b) plane for $(\phi_a, \phi_b) = (\pi, \pi)$. The black curve and the gray curve correspond to the first and the second equation of Eq. (5), respectively. The intersections of the two curves stand for the fixed points solutions. The conditions for the existence of each panel are (a) $0 < 2J < (U - U_{ab})\sqrt{(U - U_{ab})/(U + U_{ab})}$, (b) $(U - U_{ab})\sqrt{(U - U_{ab})/(U + U_{ab})} < 2J < (U - U_{ab})$, (c) $(U - U_{ab}) < 2J < (U + U_{ab})$, and (d) $2J > (U + U_{ab})$.

Equations (5) define two curves in the (z_a, z_b) plane. We plot these curves for the case of $(\phi_a, \phi_b) = (\pi, \pi)$ in Fig. 1. The four panels correspond to different values of U, U_{ab}, and J. In each panel the intersections of the two curves stand for the desired fixed point solutions. Due to the symmetry between the two species in our model, these fixed point solutions can be classified into four cases in terms of z_a and z_b: (i) $z_a = z_b = \pm\sqrt{1 - [2J/(U + U_{ab})]^2}$ when $0 \leqslant 2J < (U + U_{ab})$; (ii) $z_a = -z_b = \pm\sqrt{1 - [2J/(U - U_{ab})]^2}$ when $0 \leqslant 2J < (U - U_{ab})$; (iii) $z_a = z_b = 0$; and (iv) $|z_a| \neq |z_b|$. They are called symmetrical (S), antisymmetrical (An), isotropic (I), and asymmetrical (As) cases, respectively. The isotropic case always exists and the asymmetrical case can only be solved numerically. Note that the number of fixed points (as labeled in Fig. 1) for S, An, I, and As cases are 2, 2, 1, and 4, respectively. For given U and U_{ab}, the value of J increases from Fig. 1(a) to Fig. 1(d), and all the fixed points S, An, and As shift towards the isotropic one I and converge to I in the end.

We need to analyze the stability of fixed points in order to find out whether the requirement of adiabatic evolution of the system is fulfilled. To do this we work with the second-order differential equations of z_a and z_b. The infinitesimal variables δ_a and δ_b are introduced by $z_a = z_a^0 + \delta_a$, $z_b = z_b^0 + \delta_b$ where z_a^0 and z_b^0 satisfy Eqs. (5). According to Eqs. (3), the linearized equations of motion for $(\phi_a, \phi_b) = (\pi, \pi)$ are derived,

$$\begin{pmatrix} \ddot{\delta}_a \\ \ddot{\delta}_b \end{pmatrix} = -\Omega \begin{pmatrix} \delta_a \\ \delta_b \end{pmatrix}, \tag{6}$$

where

$$\Omega = \begin{pmatrix} 4J^2 + (Uz_a^0 + U_{ab}z_b^0)^2 - 2JU\sqrt{1-(z_a^0)^2} & -2JU_{ab}\sqrt{1-(z_a^0)^2} \\ -2JU_{ab}\sqrt{1-(z_b^0)^2} & 4J^2 + (Uz_b^0 + U_{ab}z_a^0)^2 - 2JU\sqrt{1-(z_b^0)^2} \end{pmatrix}. \tag{7}$$

The eigenvalues of Ω correspond to the square of eigenfrequencies of the system around each fixed point, which read

$$\omega_{\pm}^2 = 4J^2 + \frac{M_1^2 + M_2^2 - 2JU(Q_a + Q_b)}{2} \pm \frac{\sqrt{[(M_1^2 - M_2^2) - 2JU(Q_a - Q_b)]^2 + 16J^2U_{ab}^2Q_aQ_b}}{2}, \tag{8}$$

where $M_1 = Uz_a^0 + U_{ab}z_b^0$, $M_2 = Uz_b^0 + U_{ab}z_a^0$, $Q_a = \sqrt{1-(z_a^0)^2}$, and $Q_b = \sqrt{1-(z_b^0)^2}$.

The expressions of eigenfrequencies can be simplified if we substitute the aforementioned fixed point solutions into Eq. (8). In Table I we list the analytical expressions of eigenfrequencies and the corresponding eigenvectors for fixed points S, An, and I (that for fixed points As are unlisted because of the unavailability of their analytic solutions). There are two kinds of eigenvectors in the table: $(-1,1)$ and $(1,1)$. The former corresponds to the spin mode while the later the density mode. The two modes can be understood as in- and out-of-phase oscillations of two coupled Josephson currents [18].

The fixed points are dynamically stable as long as the corresponding frequencies ω_+ and ω_- are both real. The stability diagrams of fixed points S, An, I, and As are plotted in the (U_{ab},J) space for $(\phi_a,\phi_b)=(\pi,\pi)$ in Figs. 2(a)–2(d), respectively. In each panel the lined area corresponds to the parameter space for the existence of a fixed point, and the grayed area to the stable region. As shown in Fig. 2(a), fixed points S are always stable. For both fixed points An, and I, there exist a stable and an unstable region as represented in Figs. 2(b) and 2(c). Figure 2(d) shows that fixed points As are always unstable. They are marked, respectively, by dots and circles in Fig. 1 so as to distinguish between stable and unstable fixed points.

Until now we have focused our attention on the case of $(\phi_a,\phi_b)=(\pi,\pi)$ which is relevant to our discussion in the next section. The other three cases can be derived by means of the similar strategy which we omit here for the sake of saving space.

TABLE I. Eigenfrequencies and the corresponding eigenvectors for fixed points S, An, and I.

Fixed points	Eigenfrequencies	Eigenvectors
S	$\omega_+ = \sqrt{(U+U_{ab})^2 - 4J^2\frac{U-U_{ab}}{U+U_{ab}}}$	$(-1,1)$
	$\omega_- = \sqrt{(U+U_{ab})^2 - 4J^2}$	$(1,1)$
An	$\omega_+ = \sqrt{(U-U_{ab})^2 - 4J^2}$	$(-1,1)$
	$\omega_- = \sqrt{(U-U_{ab})^2 - 4J^2\frac{U+U_{ab}}{U-U_{ab}}}$	$(1,1)$
I	$\omega_+ = \sqrt{4J^2 - 2J(U-U_{ab})}$	$(-1,1)$
	$\omega_- = \sqrt{4J^2 - 2J(U+U_{ab})}$	$(1,1)$

IV. ADIABATIC EVOLUTION WITH HIGH-FREQUENCY PERIODIC MODULATION

The fixed points will shift accordingly in the phase space if the tunneling strength is tuned adiabatically. Instead of varying the value of J directly, we apply a high-frequency periodic modulation of the energy bias between the two wells,

$$H' = A\sin(\omega_{hf}t)\sum_{\sigma}(\hat{c}_{\sigma 1}^{\dagger}\hat{c}_{\sigma 1} - \hat{c}_{\sigma 2}^{\dagger}\hat{c}_{\sigma 2}), \tag{9}$$

where A and ω_{hf} stand for the amplitude and frequency of the modulation, respectively. After we take account of the influence of the above modulation, the equations of motion become

$$\dot{\phi}_a = J\cos(\phi_a - S)\frac{2z_a}{\sqrt{1-z_a^2}} + Uz_a + U_{ab}z_b,$$

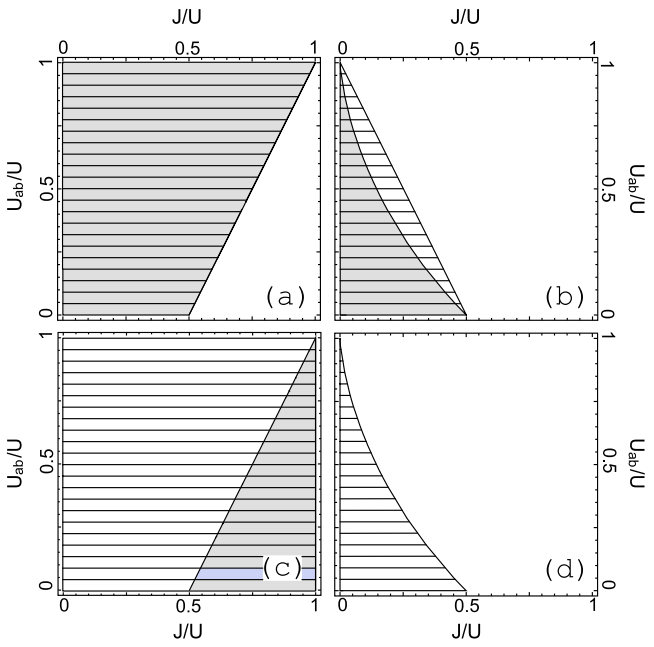

FIG. 2. (Color online) The stability diagrams of fixed points in the (U_{ab},J) space for $(\phi_a,\phi_b)=(\pi,\pi)$. Here U_{ab} and J are in units of U. Panels (a)–(d) correspond to fixed points S, An, I, and As, respectively. The lined areas refer to the parameter space for the existence of each kind of fixed points, and the grayed areas to the stable region for those fixed points accordingly.

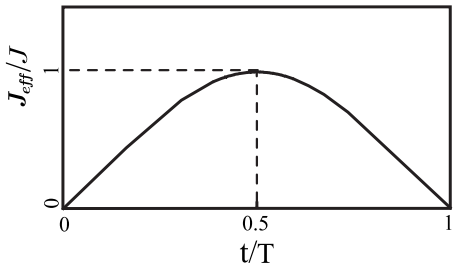

FIG. 3. Schematic plot of J_{eff} as a function of t.

$$\dot{z}_a = -2J \sin(\phi_a - S)\sqrt{1 - z_a^2},$$

$$\dot{\phi}_b = J \cos(\phi_b - S)\frac{2z_b}{\sqrt{1 - z_b^2}} + Uz_b + U_{ab}z_a,$$

$$\dot{z}_b = -2J \sin(\phi_b - S)\sqrt{1 - z_b^2}, \tag{10}$$

where $S=\frac{2A}{\omega_{hf}}\cos(\omega_{hf}t)$. In the high-frequency approximation, ω_{hf} being much lager than the intrinsic frequencies ω_+ and ω_-, the above equations reduce to a set of equations that are formally the same as Eqs. (3) with J being replaced by the effective tunneling term $J_{eff}=J\mathcal{J}_0(\frac{2A}{\omega_{hf}})$. Here $\mathcal{J}_0$ denotes the zeroth Bessel function of the first kind. Clearly, the value of J_{eff} can be tuned by varying the amplitude A.

It is interesting to consider the Rosen-Zener form of J_{eff}, i.e., J_{eff} increases from zero to its maximum value J and then decreases to zero again in the end. For pulse-shape J_{eff}, the amplitude A varies with respect to time in the following form:

$$A(t) = \begin{cases} 2.405\omega_{hf}\left(\frac{1}{2} - \frac{t}{T}\right), & \text{if } 0 \leqslant t < \frac{T}{2}, \\ 2.405\omega_{hf}\left(\frac{t}{T} - \frac{1}{2}\right), & \text{if } \frac{T}{2} \leqslant t \leqslant T, \end{cases}$$

where the coefficient 2.405 is given by the first zero point of $\mathcal{J}_0$ and T is the modulation interval. The adiabatic condition is satisfied when $T \gg \max\{1/\omega_+, 1/\omega_-\}$. Note that the precise form of A is not important as long as it satisfies the adiabatic condition; and the present form is chosen just for its simplicity. With this form of A we plot the time dependence of J_{eff} in Fig. 3.

The four panels of Fig. 2 are projected into one shown in Fig. 4. For given U and U_{ab}, the three critical tunneling strengths which divide the parameter space (U_{ab},J) into four different regions are $J_{c1}=(U-U_{ab})\sqrt{(U-U_{ab})/(U+U_{ab})}/2$, $J_{c2}=(U-U_{ab})/2$, and $J_{c3}=(U+U_{ab})/2$. In the following numerical simulation, we consider two cases for the initial states, namely, symmetrical $(z_a,z_b)=(1,1)$ and antisymmetrical $(z_a,z_b)=(1,-1)$ cases. The former state corresponds to one of fixed points S, while the latter to another fixed points An at the beginning of the evolution. The initial values of ϕ_a and ϕ_b are not well-defined for these two cases. However, as J_{eff} increases above zero adiabatically, the symmetry will be broken and the system will collapse into the $(\phi_a,\phi_b)=(\pi,\pi)$ case smoothly just like the single-species case [9];

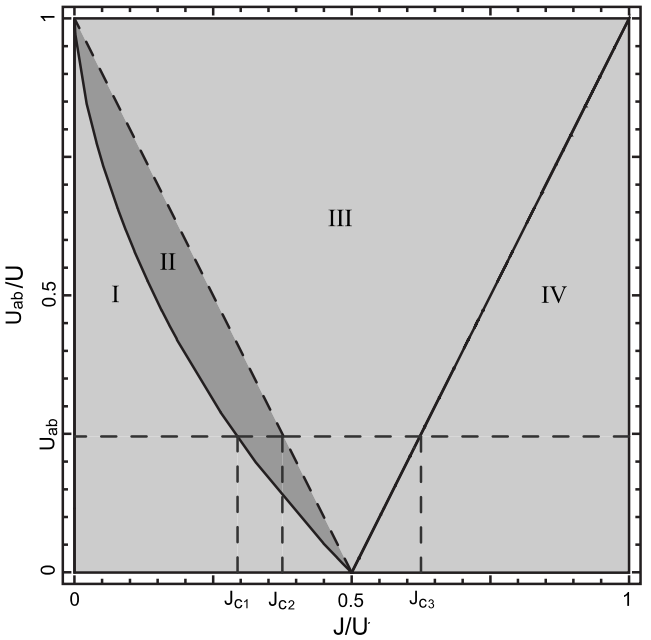

FIG. 4. Multiple stability diagram of the fixed points in the (U_{ab},J) space for $(\phi_a,\phi_b)=(\pi,\pi)$ which is formed by projecting all four panels of Fig. 2 into one. The (U_{ab},J) space is divided into four regions I–IV which correspond to Figs. 1(a)–1(d), respectively; and for given U_{ab}, there exist three critical values of J: J_{c1}, J_{c2}, and J_{c3}, accordingly.

and, if the adiabatic condition is always satisfied during the evolution, the system will remain in the $(\phi_a,\phi_b)=(\pi,\pi)$ case. That is why we only focused our attention on the $(\phi_a,\phi_b)=(\pi,\pi)$ case in the previous sections.

A. Symmetrical initial state

There exist stable fixed points S in the three regions I, II, and III shown in Fig. 4. Consequently, among the three critical tunneling strengths, only J_{c3} is related to the adiabatic evolution of fixed points S when the values of U and U_{ab} are fixed. As shown in Fig. 5, the adiabatic evolutions for $J<J_{c3}$ or $J>J_{c3}$ are quite different.

As J_{eff} increases from zero, the system evolves towards the region IV given in Fig. 4, which corresponds to the approach of fixed points S to I in Fig. 1. However, when $J<J_{c3}$, no merger between fixed points S and I occurs. When J_{eff} decreases to zero again, the system can safely remain on the fixed point and come back to the initial state smoothly. Thus there will be no population transfer as shown in Figs. 5(a) and 5(b). For $J>J_{c3}$, when J_{eff} increases above J_{c3}, the fixed points S and I merge together and the state becomes fixed point I which is stable in region IV given in Fig. 4. Additionally, when J_{eff} decreases below J_{c3}, there are some probabilities for the system to end up in $(z_a,z_b)=(-1,-1)$ which is the other S fixed point. However, as show in Figs. 5(c) and 5(d), which symmetrical final state the system will end up depends on the parameters of the system U, U_{ab}, and J as well as the external periodic modulation. Note that for the symmetrical initial state the whole evolution is just like

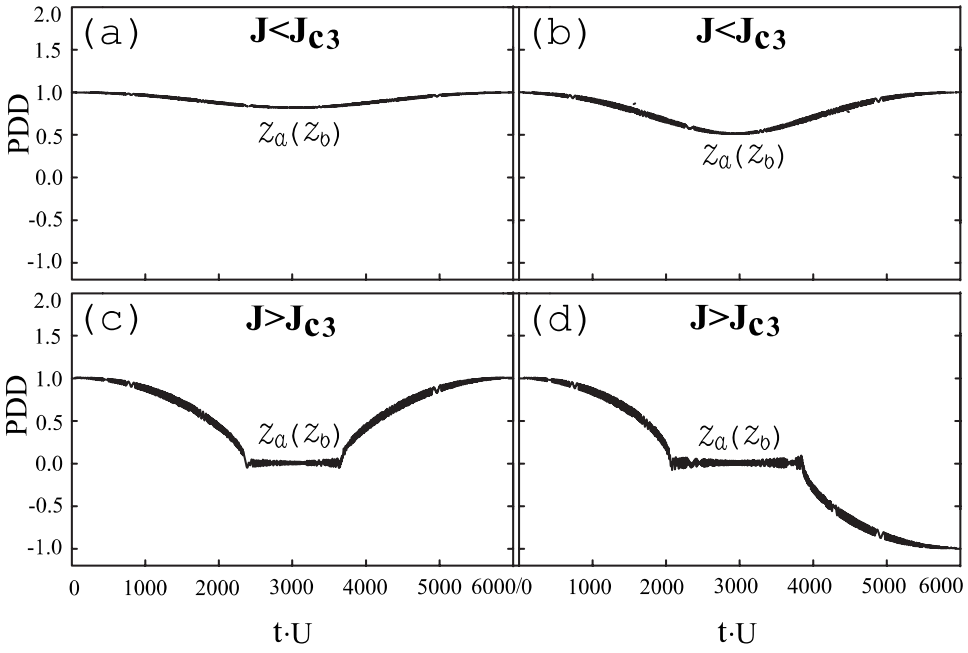

FIG. 5. Time dependence of the particle distribution difference (PDD) for each species between the two wells for the symmetrical initial state $(z_a,z_b)=(1,1)$. The parameters are $U=2$, $U_{ab}=0.4U$, $\omega_{hf}=25U$, and $T=6000/U$. In this case $J_{c3}=0.7U$. (a) $J=0.4U$, (b) $J=0.6U$, (c) $J=0.75U$, and (d) $J=0.8U$.

the single-species case [9] while the role of U is replaced by $U+U_{ab}$.

B. Antisymmetrical initial state

In contrast to the above symmetrical case, the adiabatic evolution of the particle distribution for the antisymmetrical initial state $(z_a,z_b)=(1,-1)$ is quite different. As shown in Fig. 4, the fixed point An approaches the unstable region II as J_{eff} increases from zero. However, it will not enter that region when $J<J_{c1}$. When J_{eff} decreases, the system returns to its initial state as shown in Fig. 6(b). When $J>J_{c1}$, the system enters the unstable region as J_{eff} increases above J_{c1}. If the value of U_{ab} is comparable with U, such an instability can drive the evolution to be chaotic as shown in Fig. 6(a) no matter how slow the value of A is varied. For this reason, the final state is beyond the fixed point solutions and becomes totally unpredictable. The adiabatic evolution of fixed points seemly fails for $J>J_{c1}$ since the unstable region is inevitable if $U_{ab}\neq 0$. However, when the value of U_{ab} is in the weak limit, i.e., $U_{ab}\ll U$, it can produce totally different results.

When $U_{ab}\ll U$ and $J_{c1}<J<J_{c3}$, as J_{eff} increases above J_{c1}, the tiny instability can drive the system out of its unstable state, and there are three states (two degenerate symmetrical ones S and the isotropic one I) for it to jump into. As we know that the fixed point I is also unstable in this region, the system will enter one of the stable fixed points S indicated by the arrows in Fig. 1(b). When J_{eff} decreases, the system remains in this fixed point and the two BECs will be transferred into one well at the end of the modulation. However, which well it will choose sensitively depends on the concrete parameters of which a slight difference can yield the opposite result as shown in Figs. 6(c) and 6(d). The critical value J_{c2} plays no role here. In the evolution of the particle distribution, as J_{eff} increases above J_{c1}, the system has already transitioned to one of the symmetrical fixed points and stays there.

However, if $J>J_{c3}$, all the aforementioned fixed points merge into the isotropic one I which is stable when $J_{eff}>J_{c3}$. Then when J_{eff} decreases below J_{c3} again, the system can enter either the symmetrical fixed points or antisymmetrical ones, which sensitively depends on the relevant parameters as illustrated in Figs. 6(e)–6(h).

V. SUMMARY AND DISCUSSION

We studied undistinguishable two-species BECs trapped in double wells in the mean-field approximation and obtained that there exist four types of fixed point solutions rather than two types in the single-species case. The stability of each kind of fixed points was analyzed. The effective tunneling strengths were tuned in the Rosen-Zener type with the help of high-frequency periodic modulation on the energy bias between the two wells. Furthermore, we studied the adiabatic evolution of the particle distribution difference starting from two typical initial states, symmetrical $(z_a,z_b)=(1,1)$ and antisymmetrical $(z_a,z_b)=(1,-1)$. We found that the whole adiabatic evolution is similar to the single-species case [9] for the symmetrical initial state where the role of U is replaced by $U+U_{ab}$. In contrast, for the antisymmetrical initial state, the system may encounter an unstable region in the parameter space as long as $U_{ab}\neq 0$. If the value of U_{ab} is comparable with U, the evolution will be brought into chaotic regime if the system enters the unstable region. However, in the weak limit, $U_{ab}\ll U$, the instability will break the symmetry of the system and make it evolve adiabatically into the symmetrical final states. Note that this transition will not take place if we choose the original form of tunneling strength in Ref. [9] since it will preserve the symmetry of the system.

These transitions are expected to provide a route to manipulate the BECs distribution between trapping wells if the parameters of the system are chosen accordingly, e.g., as shown in Fig. 6(c), when $J_{c1}<J<J_{c3}$, two different-species

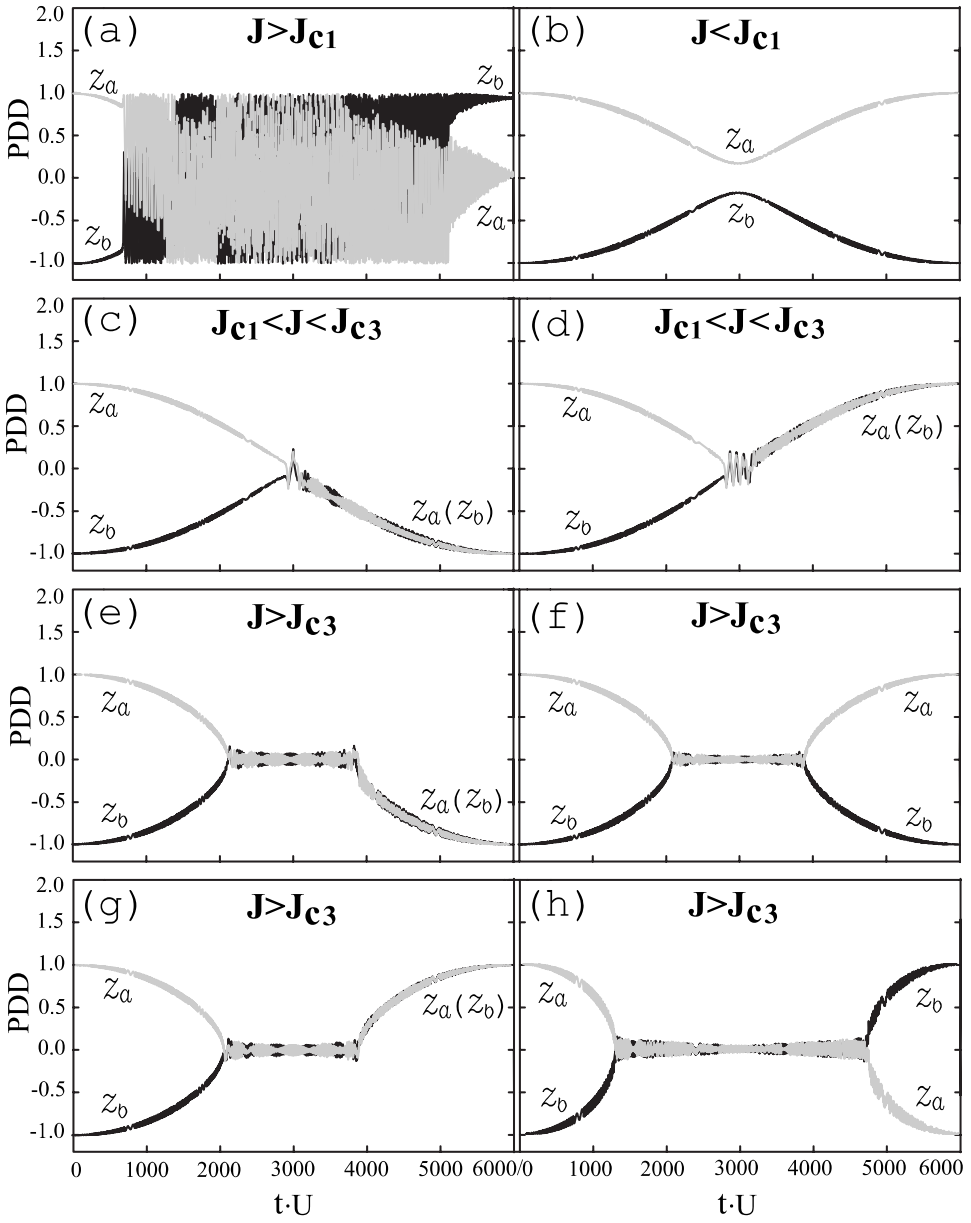

FIG. 6. Time dependence of the particle distribution difference (PDD) for each species between the two wells for the antisymmetrical initial state $(z_a, z_b) = (1, -1)$. The parameters are $U=2$, $\omega_{hf}=25U$, and $T=6000/U$. (a) $U_{ab}=0.6U$ and $J=0.35U$, (b) $U_{ab}=0.005U$ and $J=0.49U$, (c) $U_{ab}=0.005U$ and $J=0.4965U$, (d) $U_{ab}=0.005U$ and $J=0.5U$, (e) $U_{ab}=0.005U$ and $J=0.565U$, (f) $U_{ab}=0.005U$ and $J=0.57U$, (g) $U_{ab}=0.005U$ and $J=0.575U$, and (h) $U_{ab}=0.005U$ and $J=0.85U$.

BECs that are initially prepared in different wells can be transferred into the same well. However, the sensitivity of the transfer result to the precise parameters of the system should be noticed. We have numerically simulated the evolution process for a wide range of parameters. For the transition shown in Fig. 5(d), we found that a tiny variation of J, i.e., $\Delta J \simeq 0.0003U$, can produce the opposite transfer result if all other parameters are fixed. This is seemingly a challenge for experiments. We have set the value of T fixed in previous sections, whereas, if we fix the values of all other parameters but to tune the value of T, the variation of T, i.e., $\Delta T \simeq 24/U$, can also produce the opposite transfer result. For the transitions shown in Figs. 6(c)–6(h), ΔJ and ΔT are almost of the same order. In the typical BEC experiment with sodium [22], its lifetime is about 1 s, and $1/U \simeq 3.92 \times 10^{-2}$ ms; and in the typical BEC experiment with rubidium [23], its lifetime is about 15 s while $1/U \simeq 9$ ms. For both experiments, the values of T can be both less than the lifetimes, which means the experimental realization of our proposal is possible in both cases.

ACKNOWLEDGMENTS

The work was supported by NSFC Grant No. 10674117 and partially by PCSIRT Grant No. IRT0754.

[1] M. Grifoni and P. Hänggi, Phys. Rep. **304**, 229 (1998).
[2] A. Smerzi, S. Fantoni, S. Giovanazzi, and S. R. Shenoy, Phys. Rev. Lett. **79**, 4950 (1997).
[3] G. J. Milburn, J. Corney, E. M. Wright, and D. F. Walls, Phys. Rev. A **55**, 4318 (1997).
[4] S. Raghavan, A. Smerzi, S. Fantoni, and S. R. Shenoy, Phys. Rev. A **59**, 620 (1999).
[5] M. Albiez, R. Gati, J. Fölling, S. Hunsmann, M. Cristiani, and M. K. Oberthaler, Phys. Rev. Lett. **95**, 010402 (2005).
[6] K. W. Mahmud, H. Perry, and W. P. Reinhardt, Phys. Rev. A **71**, 023615 (2005).
[7] L. B. Fu and J. Liu, Phys. Rev. A **74**, 063614 (2006).
[8] N. Rosen and C. Zener, Phys. Rev. **40**, 502 (1932).
[9] D. F. Ye, L. B. Fu, and J. Liu, Phys. Rev. A **77**, 013402 (2008).
[10] N. Tsukada, M. Gotoda, Y. Nomura, and T. Isu, Phys. Rev. A **59**, 3862 (1999).
[11] A. Eckardt, T. Jinasundera, C. Weiss, and M. Holthaus, Phys. Rev. Lett. **95**, 200401 (2005).
[12] C. E. Creffield and T. S. Monteiro, Phys. Rev. Lett. **96**, 210403 (2006).
[13] T. L. Ho and V. B. Shenoy, Phys. Rev. Lett. **77**, 3276 (1996).
[14] D. S. Hall, M. R. Matthews, J. R. Ensher, C. E. Wieman, and E. A. Cornell, Phys. Rev. Lett. **81**, 1539 (1998).
[15] E. V. Goldstein, M. G. Moore, H. Pu, and P. Meystre, Phys. Rev. Lett. **85**, 5030 (2000).
[16] H. T. Ng, C. K. Law, and P. T. Leung, Phys. Rev. A **68**, 013604 (2003).
[17] L. H. Wen and J. H. Li, Phys. Lett. A **369**, 307 (2007).
[18] S. Ashhab and C. Lobo, Phys. Rev. A **66**, 013609 (2002).
[19] H. Pu, W. P. Zhang, and P. Meystre, Phys. Rev. Lett. **89**, 090401 (2002).
[20] Ö. E. Müstecaplioğlu, W. X. Zhang, and L. You, Phys. Rev. A **75**, 023605 (2007).
[21] The same strategy can be generalized to more complicated cases where the interaction strengths and tunneling of the two species are different. More richer situations are expected to appear then.
[22] K. B. Davis, M.-O. Mewes, M. R. Andrews, N. J. van Druten, D. S. Durfee, D. M. Kurn, and W. Ketterle, Phys. Rev. Lett. **75**, 3969 (1995).
[23] M. H. Anderson, J. R. Ensher, M. R. Matthews, C. E. Wieman, and E. A. Cornell, Science **269**, 198 (1995).